# Abstract

 Beyond glycemic control, SGLT2 inhibitors (SGLT2i) have protective effects on cardiorenal function. Renoprotection has been suggested to involve inhibition of NHE3 leading to reduced ATP-dependent tubular workload and mitochondrial oxygen consumption. NHE3 activity is also important for regulation of endosomal pH, but the effects of SGLT2i on endocytosis are unknown. We used a highly differentiated cell culture model of proximal tubule (PT) cells to determine the direct effects of SGLT2i on Na<sup>+</sup>-dependent fluid transport and endocytic uptake in this nephron segment. Strikingly, canagliflozin but not empagliflozin reduced fluid transport across cell monolayers, and dramatically inhibited endocytic uptake of albumin. These effects were independent of glucose and occurred at clinically relevant concentrations of drug. Canagliflozin acutely inhibited surface NHE3 activity, consistent with a direct effect, but did not affect endosomal pH or NHE3 phosphorylation. Additionally, canagliflozin rapidly and selectively inhibited mitochondrial complex I activity. Inhibition of mitochondrial complex I by metformin recapitulated the effects of canadiflozin on endocytosis and fluid transport, whereas modulation of downstream effectors AMPK and mTOR did not. Mice given a single dose of canagliflozin excreted twice as much urine over 24 h compared with empagliflozin-treated mice despite similar water intake. We conclude that canadiflozin selectively suppresses Na<sup>+</sup>-dependent fluid transport and albumin uptake in PT cells via direct inhibition of NHE3 and of mitochondrial function upstream of the AMPK/mTOR axis. These additional targets of canagliflozin contribute significantly to reduced PT Na<sup>+</sup>-dependent fluid transport in vivo.

### **New and Noteworthy**

Reduced NHE3-mediated Na<sup>+</sup> transport resulting in lower mitochondrial burden has been suggested to underlie the cardiorenal protection provided by SGLT2 inhibitors. We found that canagliflozin, but not empagliflozin, reduced NHE3-dependent fluid transport and endocytic uptake in cultured proximal tubule cells. These effects were independent of SGLT2 activity and resulted from inhibition of mitochondrial complex I and NHE3. Studies in mice are consistent with greater effects of canagliflozin vs empagliflozin on fluid transport. Our data suggest that these selective effects of canagliflozin contribute to reduced Na<sup>+</sup>-dependent transport in proximal tubule cells.

#### Introduction

A major function of the proximal tubule (PT) is the comprehensive recovery of glucose from the tubular ultrafiltrate. This is accomplished by the concerted functions of the two sodium glucose transporters SGLT2 and SGLT1, which are expressed in the S1 and S2/S3 segments of kidney PTs, respectively (1). SGLT2 functions as a low-affinity, high-capacity transporter with equimolar Na<sup>+</sup>:glucose stoichiometry. Under normal conditions, SGLT2 transport capacity is sufficient to recover nearly all of the filtered glucose. SGLT1, which maintains a 2:1 Na<sup>+</sup>:glucose stoichiometry, generally serves as a high-affinity, low-capacity reserve transporter to recover residual glucose in later PT segments. SGLT1's role in recovery increases when glucose concentrations exceed the capacity for retrieval by SGLT2, as in diabetic states (2).

SGLT2 inhibitors (SGLT2i) are a clinical game changer for the treatment of Type 2 diabetes. These drugs, known collectively as gliflozins, are structurally based on the glycoside phlorizin, and exhibit nanomolar affinity for either or both SGLTs (3, 4). Gliflozins act by competing with glucose binding to SGLTs to prevent PT glucose uptake and thus normalize plasma glucose levels. Numerous studies have demonstrated attenuated declines in kidney function and cardiovascular health in diabetic patients treated with empagliflozin, canagliflozin, dapagliflozin, or tofogliflozin, among others (5–8).

Remarkably, gliflozins also show cardiorenoprotective effects in non-diabetic individuals (9–14). In the DAPA-HF study, dapagliflozin improved heart failure outcomes and slowed progression of chronic kidney disease and death in individuals with or without diabetes (15). Cassis and colleagues similarly showed that dapagliflozin has renoprotective benefits in non-diabetic mice with progressive proteinuric nephropathy caused by repeated BSA injections (16).

The complexity of SGLT2i effects in animal models makes it challenging to determine the direct effects of SGLT2i on PT cells. SGLT2i treatment induces sustained glucosuria, diuresis, and natriuresis and induces urea transporter UT-A1 expression in the medulla to drive water reabsorption in both diabetic and normal rats (17–20). Signaling from later nephron segments, such as the macula densa, or extrarenal effects may preserve PT function by limiting GFR. Slower progression of glomerular disease and associated albuminuria may also protect PT cells from oxidative damage and other insults (14). Inhibition of PT NHE3 activity by SGLT2i has also been implicated as a protective mechanism to increase diuresis and natriuresis (17, 18). How this occurs is unknown, but it is observed in the absence of glucose and has been speculated to involve interaction of NHE3 and SGLT2 via MAP17 (21). Direct interaction of empagliflozin with NHE1 in human atrial cardiomyocytes, which do not express SGLT2, has also been reported, although recent studies argue against this possibility (22–24). Other off-target effects of some gliflozins, including activation of AMPK, have also been suggested to contribute to cardiorenal protection of this class of drugs (25–28).

A confounding issue in many studies examining the effects of treatment with SGLT2i are the relatively high concentrations of drug commonly administered to rodents, in part because of more extensive catabolism in these models (29). For example, rat studies have typically used daily oral dosages of 1.5-2 mg/kg dapagliflozin, whereas the recommended daily human dosage is ~30-fold lower (16, 30). Thus, off-target effects of gliflozins and their metabolites may contribute variably to renal and extrarenal function in cell culture, animal models, and diabetic vs nondiabetic humans.

We have developed optimized culture conditions for the opossum kidney (OK) cell line that recapitulate key morphological and functional features of the PT, including high expression of the megalin and cubilin receptors that retrieve filtered proteins from the tubule lumen, robust ion and fluid transport, and reliance on oxidative phosphorylation as a primary metabolic pathway (31, 32). These cells most closely resemble those of the PT S1 segment, based in part on their selective expression of SGLT2 (33, 34). Here we utilized this powerful and physiologically relevant system to dissect the direct and immediate effects of SGLT2i on PT cell functions.

# Results

#### A subset of SGLT2 inhibitors inhibit PT fluid transport and albumin uptake.

We compared the effects of canagliflozin and empagliflozin on Na $^+$ -dependent fluid transport across monolayers of filter-grown OK cells over a 6 h incubation. Under our culture conditions, OK cells exhibit robust apical-to-basolateral transport of fluid, amounting to ~10  $\mu$ L/h, of which roughly half is inhibited by the selective NHE3 inhibitor S3226 (Fig. 1A). S3226 has a similar maximal effect on NHE3 activity in LLC-PK<sub>1</sub> cells (35). Inhibition of the Na $^+$ K $^+$ -ATPase using ouabain (10  $\mu$ M) inhibited fluid transport by ~70% (Fig. 1A). Canagliflozin, but not empagliflozin, inhibited fluid transport across OK cell monolayers to a similar extent as S3226, and transport was not further reduced by combined addition of the two drugs (Fig. 1A). Tofogliflozin had effects similar to canagliflozin (Fig. S1A). The effects of canagliflozin on fluid transport did not depend on glucose in the media, consistent with the demonstration by Malnic and colleagues of

glucose-independent inhibition of Na<sup>+</sup> transport by phlorizin in microperfused rats [Fig. 1B; (17)]. These data suggest an SGLT2-independent mechanism.

To examine whether the different effects of canagliflozin and empagliflozin on fluid transport stemmed, at least in part, from NHE3 inhibition, we measured the effect of these drugs on intracellular pH (pHi) recovery rates after an acid load. In the presence of extracellular Na<sup>+</sup>, NHE3 accelerates pH recovery. We incubated cells overnight with each compound, induced acid loading using NH<sub>4</sub>Cl, and then measured pHi recovery rates after NH<sub>4</sub>Cl removal by fluorescence. In OK cells, canagliflozin reduced H<sup>+</sup> transport rates compared to untreated cells, and resulted in rates similar to those measured in the absence of extracellular Na<sup>+</sup> or the presence of S3226 (Fig. 2A). In contrast, recovery rates in the presence of empagliflozin were similar to untreated cells.

We also measured the acute effect of these drugs on the activity of rabbit NHE3 heterologously expressed in NHE1-null Chinese hamster ovary cells (AP-1 cells). Heterologous expression of NHE3 increased acid load pHi recovery rates and was sensitive to the NHE3 inhibitor ethylisopropylamiloride (EIPA). When we tested SGLT2 inhibitors added simultaneous to NH<sub>4</sub>Cl removal, results paralleled those in OK cells: canagliflozin reduced pH recovery rates while empagliflozin had little effect (Fig. 2B). These results suggest that canagliflozin rapidly and directly inhibits surface NHE3 from both opossum and rabbit, whereas empagliflozin does not.

Acute reductions in NHE3 activity reduce the efficiency of endocytic uptake in the PT (36–38). Confocal imaging revealed that uptake of a fluorescent albumin conjugate was considerably reduced in cells pre-treated with 25  $\mu$ M canagliflozin, but not empagliflozin (Fig. 3A). We assessed the dose-dependent effects of these drugs on albumin uptake using spectrofluorimetry. Canagliflozin inhibited albumin uptake in a dose-dependent manner, whereas empagliflozin had no effect on endocytic uptake, even at concentrations up to 50  $\mu$ M (Fig. 3B), or after 48h preincubation with 50  $\mu$ M empagliflozin (Fig. S2A). By contrast, canagliflozin inhibited albumin uptake after as little as 15 min pretreatment (Fig. S2B), and its effect was fully reversed by 45 min of washout (Fig. S2C). As with fluid transport, the effects of canagliflozin on albumin uptake were independent of glucose (Fig. 3C). Tofogliflozin also inhibited albumin uptake in a dose-dependent manner (Fig. S1B).

Addition of canagliflozin to either the apical or basolateral surface produced a partial response, suggesting that the drug acts intracellularly and gains entry from both plasma membrane domains (Fig. S3A). The organic anion transporter inhibitors probenecid and cimetidine did not blunt the effect of canagliflozin on albumin uptake, suggesting an alternative pathway for drug entry into PT cells (Fig. S3B). Because canagliflozin binds to serum proteins including albumin, we tested whether serum affected canagliflozin-inhibited uptake of dextran, a fluid-phase marker that accompanies albumin into endocytic vesicles (39). Inclusion of 5% serum with canagliflozin did not alter the inhibitory effect of 25  $\mu$ M canagliflozin on the uptake of dextran, a fluid phase marker that enters apical endocytic vesicles together with filtered ligands (Fig. S3C).

#### NHE3 inhibitors synergize with canagliflozin to impair albumin uptake.

The difference in dose dependence profiles of gliflozins on albumin uptake versus fluid transport led us to ask whether inhibition of NHE3 activity contributes to reduced albumin uptake in canagliflozin-treated cells. A role for NHE3 in PT megalin/cubilin-mediated endocytosis is well-established in cultured cells and *in vivo*. *Nhe3*<sup>-/-</sup> and heterozygous mice exhibited higher proteinuria than wild-type mice, and inhibition of NHE3 impairs endocytosis in OK cells (36, 38). Consistent with previous studies, S3226 and EIPA inhibited albumin uptake when added

individually to OK cells. However, uptake was further reduced when these were added together with canagliflozin [Fig. 4A, (37, 40)].

Pharmacologic studies suggest that NHE3 regulates membrane traffic via effects on endosomal pH, although its specific role in this process is unresolved (37, 41, 42). We used ratio imaging to measure the effects of adding canagliflozin, S3226, or both drugs together, on endosomal pH in OK cells. Canagliflozin had no effect on endosomal pH (pH 6.38 vs 6.33 in control cells, Fig. 4B), whereas S3226 reduced the pH of early endosomes to 6.12 and 6.06 in the absence or presence of canagliflozin, respectively. This suggests that NHE3 activity attenuates acidification in the PT apical endocytic pathway, as previously suggested (42).

Phosphorylation of the Ser-552 in mouse NHE3 does not affect NHE3 activity *per se* but is increased under physiological and pathological conditions where NHE3 activity is reduced (35, 43–45). EIPA and S3226 reduced NHE3 phosphorylation at this site, suggesting a compensatory response to the inhibitory action of these drugs (Fig. 4C). By contrast, canagliflozin had no effect on NHE3 phosphorylation (Fig. 4C). Similar results were obtained using tofogliflozin (Fig. S4).

Canagliflozin effects on fluid transport and albumin uptake are independent of the AMPK/mTOR axis. Canagliflozin and empagliflozin have been previously noted to increase phosphorylated AMPK levels in cells, consistent with the known role of glucose suppression in activating AMPK (25)(26, 28). Western blotting confirmed that, similar to the AMPK activator AICAR or the mTOR inhibitor rapamycin, exposure of OK cells to canagliflozin or empagliflozin for 6 h robustly increased phosphorylated AMPK levels (Fig. 5A). However, whereas canagliflozin concomitantly inhibited mTOR activity (measured as reduced phosphorylation of mTOR and its downstream effector S6), empagliflozin did not (Fig. 5A). Although AMPK and mTOR activities are usually coordinately regulated in opposing directions, AMPK activation can be uncoupled from mTOR inhibition under some conditions (46).

Treatment with AICAR (1 mM) for 6 h had no effect on either fluid transport or albumin uptake, whereas rapamycin (10  $\mu$ M) inhibited both fluid transport and uptake by 20-25% (Fig. 5B and 5C). No further reductions were observed after 24 h of treatment (not shown). We conclude that the rapid effect of canagliflozin on albumin uptake does not depend on AMPK activation or mTOR inhibition. Consistent with this, canagliflozin-mediated reductions in phosphorylated S6 (pS6) occurred more slowly than its effect on albumin uptake, as changes in pS6 levels were observed only when cells were treated with drug for >1 h (Fig. S5).

Canagliflozin inhibits mitochondrial complex I-supported respiration. The effects of canagliflozin on AMPK activity are thought to reflect upstream changes in energy levels and O<sub>2</sub> consumption mediated by inhibition of mitochondrial complex I (25, 47). Metformin, a known inhibitor of mitochondrial complex I, inhibited fluid transport (Fig. 4B) and albumin uptake to levels comparable to those in canagliflozin-treated cells [Fig. S6A, Fig. 4C; (48, 49)]. Rotenone similarly inhibited albumin uptake (Fig. S6B). To evaluate the effect of SGLT2i on mitochondrial respiratory capacity supported by complex I activity, we performed high resolution respirometry using permeabilized OK cells treated with canagliflozin or empagliflozin. NADH-dependent (complex I-supported) mitochondrial respiration was measured in the presence of pyruvate, malate, and glutamate. Prior to addition of ADP to stimulate ATP synthesis and electron transport chain activity, (referred to as state 4 or leak respiration), there were no differences in mitochondrial respiration between groups (Fig. 6). Following addition of ADP to stimulate oxidative phosphorylation and ATP synthesis, (referred to as state 3, or OXPHOS respiration), there was a significant reduction in mitochondrial respiratory rates in canagliflozin- but not

empagliflozin-treated cells compared with vehicle (Fig. 6). Maximum electron transport chain activity supported by complex I activity measured in the uncoupled state following FCCP treatment was similarly reduced in canagliflozin but not empagliflozin-treated cells (Fig. 6). Together, our data suggest that rapid changes in mitochondrial activity contribute to canagliflozin-mediated inhibition of albumin uptake and fluid transport.

Effect of a single dose of canagliflozin and empagliflozin on urine volume and albumin excretion in mice. Treatment of nondiabetic mice and humans with gliflozins increase diuresis over the short term, an effect thought to reflect inhibition of Na<sup>+</sup> reabsorption by SGLT2i to which the kidney adjusts over time. We wondered whether the distinct effects of canagliflozin and empagliflozin we observed in PT cells would translate to physiologically relevant changes in Na<sup>+</sup> reabsorption and albumin excretion in mice treated acutely with drug. To this end, 12 male mice acclimated to metabolic cages were maintained for 24 h without drug (baseline) and then given empagliflozin (10 mg/kg) or canagliflozin (50 mg/kg) by oral gavage. Water consumption was measured and urine was collected over each 24 h period for quantitation of albumin and creatinine concentrations. A week after gavage, the mice were reacclimated to metabolic cages and the treatment was repeated, but with mice receiving the other drug. Because there was some variation in baseline albumin and creatinine levels measured during the first vs second trials of the experiment, we normalized the data to average baseline levels in each trial and combined the data for statistical analysis. As shown in Table 1, mice treated with either empagliflozin or canagliflozin consumed ~40% more water over the 24 h treatment period. However, mice treated with canagliflozin excreted roughly twice as much urine during this period (~4-fold over baseline) compared with empagliflozin-treated mice (Table 1). In contrast to the well documented effect of these drugs in reducing albuminuria over long treatment periods. 24 h albumin excretion increased substantially (114 and 72% increase over baseline) in mice treated with canagliflozin or empagliflozin, respectively (Table I). Urine albumin/creatinine ratios (uACR) were unchanged under all treatment conditions, suggesting that albumin uptake efficiency remains constant, and that total urinary albumin excretion is dependent on filtration

#### **Discussion**

250

251

252

253

254255

256257

258

259

260261

262

263

264

265

266

267

268269

270

271272

273

274

275

276277

278279280

281 282

283

284 285

286

287

288

289 290

291

292

293

294

295296

297 298

299

Our studies demonstrate dramatic effects of specific gliflozins on essential functions of PT cells. We observed selective, glucose-independent inhibition of Na<sup>+</sup>-dependent fluid transport and endocytic uptake of albumin by canagliflozin and tofogliflozin, but not by empagliflozin. The effects of canagliflozin reflected a direct inhibition of surface NHE3, as well as rapid reduction in mitochondrial complex I activity. Urine volume in mice treated with a single dose of canagliflozin was double that of empagliflozin-treated mice despite comparable water intake, confirming acute physiologically relevant differences in fluid reabsorption. The results of our work have significant implications for the design and interpretation of human and animal studies aimed at deciphering the protective effects of gliflozins on both renal and extrarenal tissues.

Canagliflozin targets in PT cells. Our studies also show that while canagliflozin rapidly inhibits surface NHE3 activity, it does not alter endosomal pH. We interpret this to mean that canagliflozin readily enters the cytoplasm, but that membrane permeability requires a currently unknown transporter(s) that is absent or inactive in endosomes. Alternatively, it is possible that canagliflozin does not bind well to NHE3 at acidic pH. Future studies are clearly needed to understand this differential effect of canagliflozin on surface versus intracellular NHE3 activity.

The effects of gliflozins on NHE3 activity have previously been suggested to occur via interactions with MAP17, a protein that interacts with SGLT2, although direct evidence is lacking

(21, 50, 51). By contrast, our data here suggest that the effects of canagliflozin on surface NHE3 activity are independent of SGLT2 expression.

Beyond direct inhibition of NHE3, our studies demonstrate that the effect of canagliflozin on mitochondrial activity contributes to its effect on Na<sup>+</sup>-dependent fluid transport. The reductions we observed in fluid transport and albumin uptake were recapitulated by metformin, a known inhibitor of mitochondrial complex I, but not by AICAR or rapamycin. In longer term studies, loss of mTORC1 or prolonged inhibition of mTOR function has been associated with reduced endocytic uptake in the PT and in OK cells (32, 52, 53). We conclude that canagliflozinmediated changes in mitochondrial function and in consequent downstream effector activities likely contribute to the well-known protective effects of some gliflozins on renal and extrarenal tissues, and may explain the greater efficacy of canagliflozin over other SGLT2i in preserving kidney and cardiac function noted in some meta-analyses of clinical studies (54, 55). Metformin, which is commonly prescribed together with gliflozins, may be acting via similar mechanisms to further improve glycemic control in T2DM patients (56, 57). Thus, whereas gliflozin-mediated reductions in Na<sup>+</sup> reabsorption have been commonly suggested to protect PT cells from damage by reducing the ATP-dependent tubular workload and mitochondrial oxygen consumption, our data suggest that the opposite is also true, namely that reduced mitochondrial function in canagliflozin-treated animals may slow Na<sup>+</sup>-dependent transport along the entire nephron (58-60).

At first glance, the lack of synergy between canagliflozin and NHE3 inhibitors on fluid transport seems counterintuitive, because fluid transport in the PT and in OK cells is only partially driven by NHE3 under normal conditions. We hypothesized that reduced ATP generation in canagliflozin-treated cells lowers the driving force for Na<sup>+</sup> flux. Under these conditions, other Na<sup>+</sup>-dependent transporters can accommodate the demand when NHE3 activity is inhibited by S3226. This would not necessarily be the case when mitochondrial function is high. Moreover, the additional effect of canagliflozin on mitochondrial function provides a possible explanation for why this drug, in contrast to NHE3 inhibitors EIPA and S3226, does not alter NHE3 phosphorylation.

Gliflozin access to PT cells. Given its mechanisms of action, both tubular and plasma concentrations of canagliflozin contribute to its effect on PT cells. In order to impact mitochondrial activity and the AMPK/mTOR axis, canagliflozin presumably has to enter cells, and perhaps even concentrate there. We found that canagliflozin inhibited albumin uptake equally well when added to the apical or basolateral medium. The reported peak plasma concentration of canagliflozin in humans is 6-30 µM, although a considerable fraction of drug is bound to serum proteins and thus reaches the tubular lumen slowly (29, 61–64). On the other hand, gliflozins have been shown to accumulate in the kidney, and high concentrations may persist there even after drug clearance from the plasma. Kidney drug concentrations were 10-fold higher than the 1 µM peak plasma concentration (measured in mice given a very low dose of canagliflozin (3 mg/kg) (65)]. Even higher kidney:plasma ratios of other gliflozins have been reported in rats (66). The organic anion transporter OAT3 has previously been demonstrated to enhance the glucosuric effect of empagliflozin (67). However, inhibitors of organic anion transport did not affect canagliflozin-mediated inhibition of albumin uptake in our hands. The mechanism of canagliflozin entry into PT cells remains to be addressed.

Relevance to in vivo studies. We observed a large difference in 24 h urine excretion, despite comparable water intake, between male mice given a single oral dose of canagliflozin vs empagliflozin. Differences in drug availability or stability that affect SGLT2 activity directly are

unlikely to account for the discrepant effects at the high doses we used. Because we observed no effect of empagliflozin on fluid transport, we presume that the diuretic effect of this drug is due to downstream effects of high tubular glucose as previously suggested (68).

Reduced Na<sup>+</sup> reabsorption consequent to inhibition of both NHE3 activity and mitochondrial function presumably accounts for the two-fold greater urine output in canagliflozin-vs empagliflozin-treated mice in our study. Because these effects are independent of SGLT2 activity, Na<sup>+</sup> transport is presumably inhibited along the entire PT axis. Inhibition of SGLT1 might also contribute to the increased diuresis in canagliflozin-treated mice, as canagliflozin is the least selective inhibitor of SGLT2 (SGLT2:SGLT1 =160). Modeling studies estimate that a significant fraction of renal SGLT1 is inhibited in humans taking standard doses of canagliflozin (64, 69). Whether SGLT1 inhibition occurs under our dosing conditions is difficult to assess, and highlights the complications in interpreting studies in rodent models and humans, as well as the need for complementary studies to evaluate direct effects of these drugs in PT cells.

A slower decline in glomerular health, rather than effects of gliflozins on PT endocytic uptake is likely to be the primary reason for the slower progression of albuminuria documented in the patients with T2DM or CKD (6, 70) (5, 71). At first glance it is perhaps surprising that 24 h albumin excretion was elevated in mice given a single dose of either canagliflozin or empagliflozin, but similar results have been reported previously in rats dosed acutely with phlorizin (72). Total albumin excretion tracked closely with urine output, as the uACR remained constant. This supports the idea that the PT maintains consistent fractional retrieval of filtered albumin regardless of urinary output endocytic uptake efficiency along the PT axis. Thus, flow-dependent modulation of endocytic capacity, which we previously documented in OK cells, appears to operate in vivo, in parallel with the glomerulotubular balance mechanisms that preserve reabsorption efficiency of Na<sup>+</sup> and water (32, 73) (74).

Limitations of our study. Our study also leaves several questions unanswered. The mechanism by which canagliflozin enters cells, and how it perturbs mitochondrial complex I function remain unknown. Additionally, our studies examined only short treatment regimens and thus may not reflect longer term physiological adaptations to SGLT2i.

Our data provide foundational knowledge of how gliflozins acutely and directly affect PT function, but they are not necessarily relevant in determining best options for long term treatment. It is possible that the SGLT2-independent effects of canagliflozin we observed contribute to renal and extrarenal protection in diabetic and nondiabetic patients. Whether these potentially beneficial effects of canagliflozin outweigh other specific risks of this drug in humans remains to be determined (75). Our data also emphasize the need to consider species-specific differences in the mechanisms and efficiency of drug entry or accumulation into cells when translating studies in rodent and cell models to clinical benefit in humans. Given the enormous interest in these drugs, future studies using a variety of model systems, including OK cells, are certain to shed new light on the myriad mechanisms by which gliflozins impact cell function.

#### Methods

#### Cell culture.

Opossum kidney cells (OK-P subclone) were cultured on 10-cm dishes in DMEM/F12 (Sigma; RNBL4456) with 5% FBS and 5mM Glutamax (Gibco, 35050061) at 37°C in 5% CO<sub>2</sub>-95% air. For experiments, cells were dissociated from plates using Accutase (BD Biosciences, 561527) and seeded at 4x10<sup>5</sup> on 12-mm Transwell<sup>®</sup> inserts in 12-well dishes (Corning, 3401) with 0.5 mL and 1.5 mL of medium in the apical and basolateral chambers, respectively. After overnight

incubation, filters were transferred to an orbital platform shaker in the incubator and rotated at 146 rpm for 72 h with daily medium changes as previously described (32).

# Quantitation of fluid transport.

Duplicate filters of OK-P cells cultured as described above were quickly rinsed with serum free-DMEM/F12 medium (17 mM glucose, supplemented with 25 mM HEPES, and 5 mM Glutamax) and incubated with vehicle, SGLT2i [canagliflozin hemihydrate (Adooq Bioscience, A16817), empagliflozin (Cayman Chemical, 17375), tofogliflozin (Cayman Chemical, 23509)] and/or NHE3i [EIPA (Tocris Bioscience, 3378), S3226 (Millipore Sigma, SML1996)] added in 300 µL apical and 1 mL basolateral serum-free medium. After 6 h, the residual apical volume was carefully collected and measured. For experiments to measure the effect of 0- or 5-mM glucose on fluid transport or albumin uptake, incubations were performed in glucose-free Dulbecco's Modified Eagle's Medium (Sigma-Aldrich, D5030), supplemented with 0.2 g/L sodium bicarbonate, 25 mM HEPES, 5 mM Glutamax) or in equal volumes of this DMEM mixed with Ham's F-12 media (10 mM glucose, supplemented with 25 mM HEPES, 5 mM Glutamax, and 0.2 g/L sodium bicarbonate; Thermo Fisher, 21700). Ham's F-12 Nutrient Mix powder (Gibco, 21700075) was used to prepare Ham's F-12 media.

#### pH<sub>i</sub> recovery rate measurement.

Intracellular pH measurement in OK cells.

OK cells were seeded at 2.4x10<sup>5</sup> cells/well in a 24-well dish (Corning, 3526). After overnight incubation, the plate was transferred to an orbital platform shaker in the incubator and rotated at 146 rpm for 48 h with daily medium changes. Cells were then incubated overnight with S3226 (50 μM), canaqliflozin (25 μM), or empagliflozin (25 μM). The following day, cells were loaded with 2 µM BCECF-AM (Invitrogen, B1170) in DMEM/F12 (Sigma; RNBL4456) with 5% FBS and 5 mM Glutamax and incubated in the dark at 37°C in 5% CO<sub>2</sub>-95% air for 30 min. Prior to baseline measurements, cells were washed three times for 5 min with bicarbonate buffer pH-7.40 (25 mM NaHCO<sub>3</sub>, 115 mM NaCl, 5 mM KCL, 10 mM glucose, 1 mM MgSO<sub>4</sub>, 1 mM KHPO<sub>4</sub>, 2 mM CaCl<sub>2</sub>). Cells were then loaded with NH<sub>4</sub>Cl in HEPES buffer pH-7.4 (30 mM HEPES pH-7.4, 115 mM NaCl, 30 mM NH<sub>4</sub>Cl, 5 mM KCl, 10 mM glucose, 1 mM MgSO<sub>4</sub>, 1 mM KHPO<sub>4</sub>, 2 mM CaCl<sub>2</sub>) and incubated for 5 min at ambient temperature. An acid load recovery was then induced by replacing the NH₄Cl buffer for the control and treated cells with the HEPES buffer pH-7.4 (30 mM HEPES pH-7.4, 145 mM NaCl, 5 mM KCl, 10 mM glucose, 1 mM MgSO<sub>4</sub>, 1 mM KHPO<sub>4</sub>, 2 mM CaCl<sub>2</sub>). For the Na<sup>+</sup>-free condition, NH<sub>4</sub>Cl buffer was replaced with Na<sup>+</sup>-free HEPES buffer (30 mM HEPES pH-7.4, 145 mM NMDG<sup>+</sup>, 5 mM KCl, 10 mM glucose, 1 mM MgSO<sub>4</sub>, 1 mM KHPO<sub>4</sub>, 1.8 mM CaCl<sub>2</sub>). Another set of control cells were maintained in NH<sub>4</sub>Cl buffer. Cells were imaged every 15 seconds for 5 min throughout the protocol. A calibration curve for each well was obtained by imaging the cells in nigericin buffer [25 mM HEPES, 105] mM KCl, 1 mM MqCl<sub>2</sub> 100 µM nigericin (Invitrogen, N1495)] at the various pHs: 7.5, 7.0, and 6.5 (pH was adjusted with 10 mM KOH). The standard curve was then used to convert fluorescent signals measured during the experiment to intracellular pH (pH<sub>i</sub>). Individual recovery curves were fitted using a single exponential function (pH =  $A \cdot e^{-kt}$  + C). Initial rates were calculated using the value of the derivative (dpH/dt) at t=0 (i.e.,  $-k \cdot A$ ). Recovery curves were plotted after data for each curve were normalized to the first measurement collected following NH<sub>4</sub>CI removal.

Intracellular pH measurement in AP1 cells. NHE1-null Chinese hamster ovary cells (AP-1 cells; 4x10<sup>4</sup>/well; gift of John Orlowski, McGill University) were plated in the first two rows of a 24-well plate one day prior to transfection. Cells were co-transfected with cDNAs encoding rabbit NHE3 (gift of Mark Donowitz, Johns Hopkins School of Medicine) and BFP (blue fluorescent protein) using Lipofectamine LTX and PLUS reagent (Invitrogen, 15338100) following manufacturer's

instructions using 500 ng DNA per well. Cells were loaded with 10 µM SNARF in serum free media and incubated in the dark at 37°C for 30 min. SNARF (Molecular Probes, C1272) was used to measure intracellular pH and BFP was used to identify cells expressing NHE3. Cells were imaged using a BioTek Cytation5 and SNARF (531x/586m), TexasRed (586x/647m), and DAPI (377x/447m) cubes. Baseline measurements were made in a HEPES buffer (30 mM HEPES pH-7.4, 11 5 mM NaCl, 5 mM KCl, 10 mM glucose, 1 mM MgSO<sub>4</sub>, 1 mM KHPO<sub>4</sub>, 2 mM CaCl<sub>2</sub>) after 3x wash at 37°C for 5 min. Cells were then loaded with NH<sub>4</sub>Cl in HEPES buffer (30 mM HEPES pH-7.4, 30 mM NH<sub>4</sub>Cl, 115 mM NaCl, 5 mM KCl, 10mM glucose, 1 mM MgSO<sub>4</sub>, 1 mM KHPO<sub>4</sub>, 2 mM CaCl<sub>2</sub>). An acid load recovery was then induced by replacing the NH<sub>4</sub>Cl buffer with the HEPES buffer with or without EIPA (10 µM), canagliflozin (25 µM), or empagliflozin (50 μM). Cells were imaged approximately every 2.5 min throughout the protocol. For each condition, triplicate wells were plated for each condition and averaged for each biological replicate. A calibration curve was obtained by imaging the cells in nigericin containing buffers at the various pH's: 7.5, 7.0, and 6.5. The standard curve was then used to convert fluorescent signals measured during experiment to pH<sub>i</sub>. Individual recovery curves were fitted and plotted as described above.

### Albumin uptake.

Cells were pre-treated with drug as above and then incubated with 40  $\mu$ g/mL Alexa Fluor 647-albumin (Invitrogen, A34785) for 15 min at 37°C on an orbital shaker in the continued presence of drug. Filters were washed with cold phosphate-buffered saline containing MgCl<sub>2</sub> and CaCl<sub>2</sub> (PBS; Sigma, D8662), cut out of their inserts with a clean razorblade, and shaken at 4°C for 30 min in Eppendorf tubes containing 250  $\mu$ L detergent solution (50 mM Tris pH 8.0, 62.5 mM EDTA, 1% IGEPAL, 4 mg/mL deoxycholate) to solubilize the cells. Cell-associated fluorescence was quantified by spectrofluorimetry using the GloMax Multi-Detection System (Promega) as described previously (32).

For fluorescence imaging, filter-grown cells treated with drug and Alexa Fluor 647-albumin as above were washed twice in warm PBS and fixed in warm 4% paraformaldehyde in 100 mM sodium cacodylate, pH 7.4, 3 mm CaCl<sub>2</sub>, 3 mm MgCl<sub>2</sub>, and 3 mm KCl for 15 min at ambient temperature. After two washes in PBS, the filters were quenched in PBS/20mM Glycine/75mM ammonium chloride for 5 min, cut, and mounted onto glass slides with ProLong Glass Antifade Mountant. Cells were imaged on a Leica Stellaris-8 inverted confocal microscope using a 63X oil immersion objective. Images were collected using the same settings and processed identically using Photoshop to enhance their brightness for easier visualization.

## Quantitation of endosomal pH.

Endosomal pH in cells treated with vehicle, S3226, canagliflozin, or both drugs was quantified by ratiometric imaging as described previously (76). Briefly, cells were preincubated for 2 h with or without drugs, followed by 3 min incubation with a mixture of AlexaFluor 647 (Invitrogen, D22914) - and FITC- dextran (Invitrogen, D1820), washed, and rapidly imaged on a Leica SP8 confocal microscope using a 40x water objective (1.1 N.A.). Masks of endosomal compartments were generated from deconvolved images and overlaid onto the raw images to specifically quantify fluorescence in endosomal compartments. A calibration curve of FITC to 647 intensity ratios over a range of known pH values was generated using the intracellular pH calibration buffer kit (Invitrogen, P35379) according to manufacturer's instructions.

#### SDS-PAGE and immunoblotting.

OK cells cultured as described above were treated as indicated in figure legends. Cells were rinsed and solubilized in 250  $\mu$ L detergent solution with protease and phosphatase inhibitors (0.5  $\mu$ g/mL leupeptin, 0.7  $\mu$ g/mL pepstatin A, 40  $\mu$ M PMSF, 50 mM NaF, 15 mM sodium

pyrophosphate, and complete protease Inhibitor EDTA-Free [Roche, 04693159001; 1 tablet/10 ml of buffer]). Protein concentration was measured by Lowry assay. Equal amounts of total protein (12-15 µg/sample) were separated on 4-15% SDS-polyacrylamide gels, transferred to polyvinylidene fluoride membranes, blocked with 10% milk in Tris-buffered saline with 0.05% Tween-20 (TBST) and then incubated at 4°C overnight with the following primary antibodies: NHE3 (1:10, 3H3 hybridoma, graciously provided by Orson Moe, UTSW), anti-phospho-Ser552 NHE3 (1:3000, Sigma Aldrich; MABN2415), phospho-S6 (1:1000, Cell Signaling Technology; 2211), β-tubulin (1:500, Cell Signaling Technology; 86298), phospho-AMPK (1:1000, Cell Signaling Technology, 2535), AMPKa (1:1000, Cell Signaling Technology, 2532), mTOR (1:1000, Cell Signaling Technology, 2983), and phospho-mTOR (Ser2448) (1:1000, Cell Signaling Technology, 5536). The membranes were washed 3 times with TBST prior to incubation for 1 h with horseradish peroxidase-conjugated goat anti-mouse IgG (1:10,000, Jackson ImmunoResearch, 115-035-166) or peroxidase-conjugated goat anti-Rabbit IgG (1:10,000, Jackson ImmunoResearch, 111-035-144) and detected with chemiluminescence. All blots were imaged using the Bio-Rad ChemiDoc Touch Imaging System, and bands were quantitated using the Bio-Rad Image Lab software.

## Mitochondrial respirometry.

Cells were seeded at  $1.6 \times 10^6$  on 24-mm Transwell® inserts in 6-well dishes (Corning, 3412) with 1.5 mL and 2.0 mL of medium in the apical and basolateral chambers, respectively. After overnight incubation, filters were transferred to an orbital platform shaker in the incubator and rotated at 146 rpm for 72 h with daily medium changes as previously described (32). Following 72 h incubation, cells were pre-treated with or without canagliflozin (25  $\mu$ M) or empagliflozin (25  $\mu$ M) for 30 min at 37°C on an orbital shaker. Cells were then disassociated from filter supports using Accutase and total cell count and viability were assessed with Trypan blue (Sigma T-0776). Next, cells were resuspended in mitochondrial respiration medium (MiR05) (Oroboros) in the presence or absence of drug.

Mitochondrial respiration was assessed in digitonin-permeabilized OK cells using an Oroboros O2K High-Resolution Respirometer. Respirometry was performed in MiR05 at 37°C under constant mixing in a sealed, 2-ml chamber containing  $1x10^6$  OK cells/ml. The respirometry protocol consisted of sequential additions of substrates, uncouplers, and inhibitors using corresponding Hamilton syringes for manual titrations as follows: digitonin (16.2  $\mu$ M); complex 1 substrates pyruvate (5 mM), malate (2 mM), and glutamate (10 mM); adenosine diphosphate (ADP, 0.5 mM); cytochrome C (10  $\mu$ M); carbonyl cyanide 4-(trifluoromethoxy); phenylhydrazone (FCCP; titrations of 0.5  $\mu$ M until maximal respiration reached); rotenone (0.5  $\mu$ M); and antimycin A (2.5  $\mu$ M) (77). Protein concentration of the permeabilized cells was determined by BCA protein assay (Fisher Scientific, 23227), and oxygen flux was expressed per mg protein. Assays were done in the continued presence or absence of drug.

Effects of canagliflozin and empagliflozin on urine output and albumin excretion in mice.

All experimental procedures conform to the NIH Guide for the Care and Use of Laboratory Animals and were approved by the Institutional Animal Care and Use Committee of the University of Pittsburgh (IACUC approval no. 21079537). Ten-week-old male C57BL/6 mice (n=12) acclimated to metabolic cages for 24 h without drug (baseline) and then given empagliflozin (10 mg/kg) or canagliflozin (50 mg/kg) by oral gavage. Water consumption was measured daily, and urine was collected over the 24 h period prior to and after drug treatment. Albumin levels in diluted urine samples (1:500) were measured by ELISA according to the protocol provided by the discontinued mouse albumin ELISA kit from Bethyl Laboratories (Worthington, TX) and using the same primary and secondary antibodies [affinity-purified goat anti-mouse albumin antibody (Fisher Scientific, NC9197876) and HRP-conjugated detection

antibody (Fisher Scientific, NC9617149)]. Creatinine levels were quantitated using the Creatinine Enzymatic Reagent Set (Pointe Scientific C7548-480, creatinine standard: C7513-STD). Albumin/creatinine ratios were calculated as albumin (mg)/creatinine (mg) for each sample.

558 559 560

555

556 557

#### Statistics.

Experimental data were analyzed using one-way ANOVA in GraphPad Prism with additional tests as noted. P- value ≤ 0.05 was considered statistically significant.

562563564

565 566

561

### **Acknowledgements**

- We thank Mark Donowitz (Johns Hopkins School of Medicine) for providing rabbit NHE3 cDNA.
- AP-1 cells were a gift to KAW from John Orlowski (McGill University). OAW is indebted to
- Thomas Maack for his many insightful comments on the manuscript.

568 569

Table I. Single dose effects of canagliflozin and empagliflozin on urine output and albumin excretion in mice.

	Baseline (normalized)	Empagliflozin- treated (norm to baseline)	Baseline (normalized)	Canagliflozin- treated (norm to baseline)	P value cana vs empa
Water intake/24h	100+/-35.9	138.5+/-63.8	100+/-27.8	144+/-44.3	NS (0.996)
Urine output/24h	100+/-54.7	194+/-88.8 ****	100+/-63.6	409+/-201 ****	* (0.03)
Albumin/24h	100+/-31.0	172+/-67.8 ***	100+/-60.8	214+/-96.1 ***	NS (0.699)
Creatinine/24h	100+/-39.0	180+/-78.6 ***	100+/-60.6	229+/-116 ***	NS (0.710)
Albumin/Creatinine	100+/-25.6	92.9+/-21.5	100+/-32.3	96.6+/-25.4	NS (0.995)

\*\*\*p<0.001, \*\*\*\*p<0.0001 vs baseline by two-way ANOVA with Tukey's multiple comparisons test. All baseline comparisons NS except urine output p 0.03. n=12 mice per condition, two trials per mouse.

## Figure Legends

Figure 1. Canagliflozin inhibits fluid transport across PT cell monolayers in a glucose-independent manner. (A) Filter-grown OK cells were pretreated with vehicle (Ctrl) with the indicated concentrations of canagliflozin (cana) or empagliflozin (empa), or with S3226 (30  $\mu$ M) plus or minus canagliflozin (25  $\mu$ M) for 6 h. The volume of apical fluid remaining above the cells was measured and normalized to that of untreated controls in each experiment. Average fluid transport in control cells was 10.3+/- 1.57  $\mu$ L/h. (B) Cells were incubated for 6 h with or without canagliflozin (25  $\mu$ M) in medium containing the indicated concentration of glucose. Fluid transport was quantified as in panel A and normalized to control conditions (17 mM glucose). Each point in panels A and B represents data from an individual experiment where the average of replicate values was normalized to the control uptake. Statistical significance was determined by ordinary one-way ANOVA with Dunnett's multiple comparisons test in panel A and with Sidak's multiple comparisons test in panel B. Asterisks above each column denote significance relative to control (\* p<0.05, \*\*<0.01, \*\*\*<0.001, \*\*\*<0.0001).

Figure 2. Canagliflozin inhibits endogenous and heterologously expressed NHE3. (A) OK cells cultured on 24-well plates were incubated overnight with S3226 (50 µM), canagliflozin (cana, 25 μM), or empagliflozin (empa, 25 μM), and drugs were included in subsequent steps. The following day, cells were loaded with 2 µM BCECF for 30 min, and subjected to acid load as described in Methods. The acid load buffer was aspirated and intracellular pH (pHi) recovery was monitored under control or Na<sup>+</sup>-free conditions. (B) Individual recovery curves were calculated as mentioned in the methods. Each point in panel B represents data from an individually calibrated well (n=8). Statistical significance was determined by ordinary one-way ANOVA with Dunnett's multiple comparisons test. (C) AP-1 cells transfected with rabbit NHE3 cDNA as described in Methods were loaded with 10 µM SNARF for 30 min. After baseline measurements and incubation with NH<sub>4</sub>CI, acid load recovery was induced by replacing the NH<sub>4</sub>Cl buffer with the HEPES buffer with or without drug [EIPA (10 μM), canagliflozin (25 μM), or empagliflozin (50 µM)]. (D) Individual recovery curves were calculated as described in Methods. All technical replicates from three independent experiments are shown. Statistical significance was determined by ordinary one-way ANOVA with Dunnett's multiple comparisons test.

Figure 3. Glucose-independent inhibition of albumin uptake in PT cells by canagliflozin. (A) Filter-grown OK cells were pretreated for 2 h with vehicle or with canagliflozin (cana, 25 μM), or empagliflozin (empa, 25 μM), then incubated with apically added AlexaFluor-647 albumin (40 μg/mL) for 15 min before fixing and imaging. Representative fields are shown. Scale bar: 25 μm. (B) OK cells were pretreated for 6 h with vehicle (Ctrl) or with the indicated concentrations of canagliflozin or empagliflozin, and then incubated for 15 min with AlexaFluor-647 albumin prior to quantifying cell-associated albumin by spectrofluorimetry. (C) Cells were preincubated for 6 h with or without canagliflozin (25 μM) in medium containing the indicated concentration of glucose and albumin uptake measured as in panel B. Each point in panels B and C represents data from an individual experiment where the average of replicate values was normalized to the control uptake. Statistical significance was determined by ordinary one-way ANOVA with Dunnett's multiple comparisons test in B and with Sidak's multiple comparisons test in C Asterisks above each column denote significance relative to control (\*\*\*\*p<0.0001).

Figure 4. Inhibition of albumin uptake by canagliflozin is independent of NHE3. (A) Duplicate filters of OK cells were incubated for 6 h with NHE3 inhibitors EIPA (25  $\mu$ M) or S3226 (30  $\mu$ M) in the presence or absence of canagliflozin (cana, 25  $\mu$ M) before quantitation of albumin uptake. Statistical significance was determined by ordinary one-way ANOVA with Tukey's multiple comparisons test multiple comparisons. Asterisks above each bar represent

significance relative to control and horizontal bars denote statistically significant differences between other conditions (\*p<0.05, \*\*p<0.01, \*\*\*p<0.001, \*\*\*\*p<0.0001). (B) Duplicate filters of OK cells were treated for 2 h with vehicle (control), canagliflozin (25  $\mu$ M), S3226 (30  $\mu$ M), or both drugs, and the pH of early endosomes was quantified by ratio imaging as described in Methods. Each point represents a single endosome and the mean +/- SEM (in gray) for each condition is plotted (\*\*\*p<0.001, \*\*\*\*p<0.0001 by two-way ANOVA with Tukey's multiple comparisons test.) (C) Duplicate filters of OK cells were incubated with EIPA (25  $\mu$ M), S3226 (30  $\mu$ M), or canagliflozin (25  $\mu$ M) for 6 h, then solubilized. Equal protein loads were western blotted with antibodies against NHE3 and phospho-S580 NHE3 (pNHE3). A representative gel is shown. Migration of molecular mass standards (in kDa) is indicated on the right. (D) The ratio of pNHE3/NHE3 (control ratios normalized to 100% in each experiment) from 3-4 independent experiments for each condition is plotted. \*p<0.05 by one-way ANOVA vs control.

 (\*\* p< 0.01, \*\*\*p<0.001, \*\*\*\*p<0.0001).

Figure 5. Canagliflozin inhibition of albumin uptake is independent of the AMPK/mTOR axis. (A) Duplicate filters of OK cells were treated with vehicle (Ctrl), S3226 (30 μM), canagliflozin (cana, 25 μM), empagliflozin (empa, 25 μM), rapamycin (rapa, 10 μM), or AICAR (1 mM) for 6h, and then solubilized. Equal protein loads were blotted to detect AMPK and phospho-AMPK (p-AMPK) mTOR, phospho-mTOR (pmTOR), and phospho-S6 (pS6). Migration of molecular mass standards (in kDa) is indicated on the right. Similar results were obtained in three independent experiments. Duplicate filters of OK cells were treated with vehicle (Ctrl), canagliflozin (25 μM), AICAR (1 mM), rapamycin (10 μM), or metformin (met, 1 mM) for 6 h and (B) fluid transport or (C) albumin uptake was quantified. Each point represents data from an individual experiment where the average of replicate values was normalized to the control uptake. Statistical significance was determined by ordinary one-way ANOVA with Dunnett's

multiple comparisons test. Asterisks above each column denote significance relative to control

Figure 6. Canagliflozin selectively inhibits mitochondrial complex I activity. Filter-grown OK cells were pre-treated with or without canagliflozin (25 μM) or empagliflozin (25 μM) for 30 min. Mitochondrial respiration was measured in the continued presence of drug as described in Methods. State 4 represents routine respiration in the presence of complex I substrates, State 3 represents complex I ADP-stimulated activity (OXPHOS), and Max ETC represents the maximum electron transport chain activity supported by complex I activity measured in the presence of the uncoupler FCCP. Data from five independent experiments are plotted. Significance was assessed by two-way ANOVA with Dunnett's multiple comparisons test (\*\*\*\*\*p<0.0001).

673	
674	References

675 676

- Limbutara K, Chou C-L, Knepper MA. Quantitative proteomics of all 14 renal tubule segments in rat. *J Am Soc Nephrol* 31: 1255–1266, 2020. https://doi.org/10.1681/ASN.2020010071.
- Shepard BD, Pluznick JL. Saving the sweetness: renal glucose handling in health and disease. *Am J Physiol Renal Physiol* 313: F55–F61, 2017. https://doi.org/10.1152/ajprenal.00046.2017.
- Fonseca-Correa JI, Correa-Rotter R. Sodium-Glucose Cotransporter 2 Inhibitors
   Mechanisms of Action: A Review. Front Med (Lausanne) 8: 777861, 2021.
   https://doi.org/10.3389/fmed.2021.777861.
- 4. Rieg T, Vallon V. Development of SGLT1 and SGLT2 inhibitors. *Diabetologia* 61: 2079–2086, 2018. https://doi.org/10.1007/s00125-018-4654-7.
- Perkovic V, Jardine MJ, Neal B, Bompoint S, Heerspink HJL, Charytan DM,
   Edwards R, Agarwal R, Bakris G, Bull S, Cannon CP, Capuano G, Chu PL, de
   Zeeuw D, Greene T, Levin A, Pollock C, Wheeler DC, Yavin Y, Zhang H, Zinman B,
   Meininger G, Brenner BM, Mahaffey KW, CREDENCE Trial Investigators.
   Canagliflozin and renal outcomes in type 2 diabetes and nephropathy. N Engl J Med 380:
   2295–2306, 2019. https://doi.org/10.1056/NEJMoa1811744.
- 6. Wanner C, Inzucchi SE, Lachin JM, Fitchett D, von Eynatten M, Mattheus M,
  Johansen OE, Woerle HJ, Broedl UC, Zinman B, EMPA-REG OUTCOME
  Investigators. Empagliflozin and progression of kidney disease in type 2 diabetes. *N*Engl J Med 375: 323–334, 2016. https://doi.org/10.1056/NEJMoa1515920.
- Wiviott SD, Raz I, Bonaca MP, Mosenzon O, Kato ET, Cahn A, Silverman MG,
   Zelniker TA, Kuder JF, Murphy SA, Bhatt DL, Leiter LA, McGuire DK, Wilding JPH,
   Ruff CT, Gause-Nilsson IAM, Fredriksson M, Johansson PA, Langkilde A-M,
   Sabatine MS, DECLARE-TIMI 58 Investigators. Dapagliflozin and cardiovascular
   outcomes in type 2 diabetes. N Engl J Med 380: 347–357, 2019.
   https://doi.org/10.1056/NEJMoa1812389.
- Heerspink HJL, Karasik A, Thuresson M, Melzer-Cohen C, Chodick G, Khunti K,
   Wilding JPH, Garcia Rodriguez LA, Cea-Soriano L, Kohsaka S, Nicolucci A,
   Lucisano G, Lin F-J, Wang C-Y, Wittbrodt E, Fenici P, Kosiborod M. Kidney
   outcomes associated with use of SGLT2 inhibitors in real-world clinical practice (CVD-REAL 3): a multinational observational cohort study. *Lancet Diabetes Endocrinol* 8: 27–35, 2020. https://doi.org/10.1016/S2213-8587(19)30384-5.
- Dominguez Rieg JA, Xue J, Rieg T. Tubular effects of sodium-glucose cotransporter 2 inhibitors: intended and unintended consequences. *Curr Opin Nephrol Hypertens* 29: 523–530, 2020. https://doi.org/10.1097/MNH.0000000000000632.
- 713 10. **Marton A, Kaneko T, Kovalik J-P, Yasui A, Nishiyama A, Kitada K, Titze J**. Organ 714 protection by SGLT2 inhibitors: role of metabolic energy and water conservation. *Nat Rev* 715 *Nephrol* 17: 65–77, 2021. https://doi.org/10.1038/s41581-020-00350-x.

- 716 11. **Vallon V, Verma S**. Effects of SGLT2 inhibitors on kidney and cardiovascular function. 717 Annu Rev Physiol 83: 503–528, 2021. https://doi.org/10.1146/annurev-physiol-031620-095920.
- 719 12. **Wright EM**. SGLT2 inhibitors: physiology and pharmacology. *Kidney360* 2: 2027–2037, 2021. https://doi.org/10.34067/KID.0002772021.
- 13. Liu J, Tian J, Sodhi K, Shapiro JI. The Na/K-ATPase Signaling and SGLT2 Inhibitor Mediated Cardiorenal Protection: A Crossed Road? *J Membr Biol* 254: 513–529, 2021.
   https://doi.org/10.1007/s00232-021-00192-z.
- Thomson SC, Vallon V. Renal Effects of Sodium-Glucose Co-Transporter Inhibitors. *Am J Cardiol* 124 Suppl 1: S28–S35, 2019. https://doi.org/10.1016/j.amjcard.2019.10.027.
- 726
   727
   728
   729
   729
   720
   720
   721
   722
   723
   724
   725
   726
   727
   728
   729
   729
   720
   720
   720
   720
   721
   722
   723
   724
   725
   726
   727
   728
   728
   728
   728
   733
   728
   729
   720
   720
   720
   720
   720
   720
   720
   720
   720
   720
   720
   720
   720
   720
   720
   720
   720
   720
   720
   720
   720
   720
   720
   720
   720
   720
   720
   720
   720
   720
   720
   720
   720
   720
   720
   720
   720
   720
   720
   720
   720
   720
   720
   720
   720
   720
   720
   720
   720
   720
   720
   720
   720
   720
   720
   720
   720
   720
   720
   720
   720
   720
   720
   720
   720
   720
   720
   720
   720
   720
   720
   720
   720
   720
   720
   720
   720
   720
   720
   720
   720
   720
   720
   720
   720
- 730 16. Cassis P, Locatelli M, Cerullo D, Corna D, Buelli S, Zanchi C, Villa S, Morigi M,
   731 Remuzzi G, Benigni A, Zoja C. SGLT2 inhibitor dapagliflozin limits podocyte damage in proteinuric nondiabetic nephropathy. *JCI Insight* 3, 2018.
   733 https://doi.org/10.1172/jci.insight.98720.
- 734 17. **Pessoa TD, Campos LCG, Carraro-Lacroix L, Girardi ACC, Malnic G.** Functional role of glucose metabolism, osmotic stress, and sodium-glucose cotransporter isoformmediated transport on Na+/H+ exchanger isoform 3 activity in the renal proximal tubule. *J Am Soc Nephrol* 25: 2028–2039, 2014. https://doi.org/10.1681/ASN.2013060588.
- T38
   Borges-Júnior FA, Silva Dos Santos D, Benetti A, Polidoro JZ, Wisnivesky ACT,
   Crajoinas RO, Antônio EL, Jensen L, Caramelli B, Malnic G, Tucci PJ, Girardi ACC.
   Empagliflozin Inhibits Proximal Tubule NHE3 Activity, Preserves GFR, and Restores
   Euvolemia in Nondiabetic Rats with Induced Heart Failure. *J Am Soc Nephrol* 32: 1616–1629, 2021. https://doi.org/10.1681/ASN.2020071029.
- Onishi A, Fu Y, Darshi M, Crespo-Masip M, Huang W, Song P, Patel R, Kim YC,
   Nespoux J, Freeman B, Soleimani M, Thomson S, Sharma K, Vallon V. Effect of renal tubule-specific knockdown of the Na+/H+ exchanger NHE3 in Akita diabetic mice. *Am J Physiol Renal Physiol* 317: F419–F434, 2019.
   https://doi.org/10.1152/ajprenal.00497.2018.
- 748 20. Chen L, LaRocque LM, Efe O, Wang J, Sands JM, Klein JD. Effect of dapagliflozin treatment on fluid and electrolyte balance in diabetic rats. *Am J Med Sci* 352: 517–523, 2016. https://doi.org/10.1016/j.amjms.2016.08.015.
- Coady MJ, El Tarazi A, Santer R, Bissonnette P, Sasseville LJ, Calado J, Lussier Y,
   Dumayne C, Bichet DG, Lapointe J-Y. MAP17 is a necessary activator of renal
   na+/glucose cotransporter SGLT2. *J Am Soc Nephrol* 28: 85–93, 2017.
   https://doi.org/10.1681/ASN.2015111282.
- 755
   756
   757
   758
   759
   750
   751
   752
   753
   754
   755
   756
   757
   757
   758
   759
   750
   750
   751
   752
   753
   754
   755
   756
   757
   757
   758
   759
   750
   750
   750
   750
   750
   750
   750
   750
   750
   750
   750
   750
   750
   750
   750
   750
   750
   750
   750
   750
   750
   750
   750
   750
   750
   750
   750
   750
   750
   750
   750
   750
   750
   750
   750
   750
   750
   750
   750
   750
   750
   750
   750
   750
   750
   750
   750
   750
   750
   750
   750
   750
   750
   750
   750
   750
   750
   750
   750
   750
   750
   750
   750
   750
   750
   750
   750
   750
   750
   750
   750
   750
   750
   750
   750
   750
   750
   750
   750
   750
   750
   750
   750
   750
   750
   750
   750
   750
   750
   750
   750
   750

- Chung YJ, Park KC, Tokar S, Eykyn TR, Fuller W, Pavlovic D, Swietach P, Shattock
   MJ. Off-target effects of sodium-glucose co-transporter 2 blockers: empagliflozin does not inhibit Na+/H+ exchanger-1 or lower [Na+]i in the heart. *Cardiovasc Res* 117: 2794–2806, 2021. https://doi.org/10.1093/cvr/cvaa323.
- 762 24. Uthman L, Baartscheer A, Bleijlevens B, Schumacher CA, Fiolet JWT, Koeman A,
   763 Jancev M, Hollmann MW, Weber NC, Coronel R, Zuurbier CJ. Class effects of SGLT2
   764 inhibitors in mouse cardiomyocytes and hearts: inhibition of Na+/H+ exchanger, lowering
   765 of cytosolic Na+ and vasodilation. *Diabetologia* 61: 722–726, 2018.
   766 https://doi.org/10.1007/s00125-017-4509-7.
- 767
   768
   769
   760
   761
   762
   763
   764
   765
   765
   766
   766
   767
   768
   769
   760
   760
   760
   760
   760
   760
   760
   760
   760
   760
   760
   760
   760
   760
   760
   760
   760
   760
   760
   760
   760
   760
   760
   760
   760
   760
   760
   760
   760
   760
   760
   760
   760
   760
   760
   760
   760
   760
   760
   760
   760
   760
   760
   760
   760
   760
   760
   760
   760
   760
   760
   760
   760
   760
   760
   760
   760
   760
   760
   760
   760
   760
   760
   760
   760
   760
   760
   760
   760
   760
   760
   760
   760
   760
   760
   760
   760
   760
   760
   760
   760
   760
   760
   760
   760
   760
   760
   760
   760
   760
   760
   760
   760
   760
   760
   760
   760
   760
   760
   760
   760
   760
   760
   760
   760
- Park CH, Lee B, Han M, Rhee WJ, Kwak MS, Yoo T-H, Shin J-S. Canagliflozin
   protects against cisplatin-induced acute kidney injury by AMPK-mediated autophagy in
   renal proximal tubular cells. *Cell Death Discov* 8: 12, 2022.
   https://doi.org/10.1038/s41420-021-00801-9.
- Villani LA, Smith BK, Marcinko K, Ford RJ, Broadfield LA, Green AE, Houde VP,
   Muti P, Tsakiridis T, Steinberg GR. The diabetes medication Canagliflozin reduces
   cancer cell proliferation by inhibiting mitochondrial complex-I supported respiration. *Mol Metab* 5: 1048–1056, 2016. https://doi.org/10.1016/j.molmet.2016.08.014.
- Shoda K, Tsuji S, Nakamura S, Egashira Y, Enomoto Y, Nakayama N, Shimazawa
   M, Iwama T, Hara H. Canagliflozin inhibits glioblastoma growth and proliferation by activating AMPK. *Cell Mol Neurobiol* 43: 879–892, 2023. https://doi.org/10.1007/s10571-022-01221-8.
- 783 29. **Mamidi RNVS, Cuyckens F, Chen J, Scheers E, Kalamaridis D, Lin R, Silva J, Sha**784 **S, Evans DC, Kelley MF, Devineni D, Johnson MD, Lim HK**. Metabolism and excretion of canagliflozin in mice, rats, dogs, and humans. *Drug Metab Dispos* 42: 903–916, 2014. https://doi.org/10.1124/dmd.113.056440.
- 787
   788
   789
   790
   Kravtsova O, Bohovyk R, Levchenko V, Palygin O, Klemens CA, Rieg T,
   Staruschenko A. SGLT2 inhibition effect on salt-induced hypertension, RAAS, and Na+transport in Dahl SS rats. Am J Physiol Renal Physiol 322: F692–F707, 2022.
   https://doi.org/10.1152/ajprenal.00053.2022.
- 791 31. Ren Q, Gliozzi ML, Rittenhouse NL, Edmunds LR, Rbaibi Y, Locker JD, Poholek
  792 AC, Jurczak MJ, Baty CJ, Weisz OA. Shear stress and oxygen availability drive
  793 differential changes in opossum kidney proximal tubule cell metabolism and endocytosis.
  794 *Traffic* 20: 448–459, 2019. https://doi.org/10.1111/tra.12648.
- Jackson EK, Shipman KE, Rbaibi Y, Menshikova EV, Ritov VB, Eshbach ML, Jiang Y, Jackson EK, Baty CJ, Weisz OA. Proximal tubule apical endocytosis is modulated by fluid shear stress via an mTOR-dependent pathway. *Mol Biol Cell* 28: 2508–2517, 2017. https://doi.org/10.1091/mbc.E17-04-0211.
- 799 33.
   Park HJ, Fan Z, Bai Y, Ren Q, Rbaibi Y, Long KR, Gliozzi ML, Rittenhouse N,
   Locker JD, Poholek AC, Weisz OA. Transcriptional Programs Driving Shear Stress Induced Differentiation of Kidney Proximal Tubule Cells in Culture. Front Physiol 11:
   587358, 2020. https://doi.org/10.3389/fphys.2020.587358.

- Long KR, Rbaibi Y, Bondi CD, Ford BR, Poholek AC, Boyd-Shiwarski CR, Tan RJ,
   Locker JD, Weisz OA. Cubilin-, megalin-, and Dab2-dependent transcription revealed by
   CRISPR/Cas9 knockout in kidney proximal tubule cells. *Am J Physiol Renal Physiol* 322:
   F14–F26, 2022. https://doi.org/10.1152/ajprenal.00259.2021.
- 807 35. **Carraro-Lacroix LR, Malnic G, Girardi ACC**. Regulation of Na+/H+ exchanger NHE3 808 by glucagon-like peptide 1 receptor agonist exendin-4 in renal proximal tubule cells. *Am J Physiol Renal Physiol* 297: F1647-55, 2009. https://doi.org/10.1152/ajprenal.00082.2009.
- 810 36. Gekle M, Völker K, Mildenberger S, Freudinger R, Shull GE, Wiemann M. NHE3
   811 Na+/H+ exchanger supports proximal tubular protein reabsorption in vivo. Am J Physiol
   812 Renal Physiol 287: F469-73, 2004. https://doi.org/10.1152/ajprenal.00059.2004.
- 37. **Gekle M, Drumm K, Mildenberger S, Freudinger R, Gassner B, Silbernagl S.**Inhibition of Na+-H+ exchange impairs receptor-mediated albumin endocytosis in renal proximal tubule-derived epithelial cells from opossum. *J Physiol (Lond)* 520 Pt 3: 709–721, 1999. https://doi.org/10.1111/j.1469-7793.1999.00709.x.
- 38. **Gekle M**, **Freudinger R**, **Mildenberger S**. Inhibition of Na+-H+ exchanger-3 interferes with apical receptor-mediated endocytosis via vesicle fusion. *J Physiol (Lond)* 531: 619–629, 2001. https://doi.org/10.1111/j.1469-7793.2001.0619h.x.
- 820 39. **Rbaibi Y, Long KR, Shipman KE, Ren Q, Baty CJ, Kashlan OB, Weisz OA**. Megalin, cubilin, and Dab2 drive endocytic flux in kidney proximal tubule cells. *Mol Biol Cell* 34: ar74, 2023. https://doi.org/10.1091/mbc.E22-11-0510.
- Wang Y, Cai H, Cebotaru L, Hryciw DH, Weinman EJ, Donowitz M, Guggino SE,
   Guggino WB. CIC-5: role in endocytosis in the proximal tubule. *Am J Physiol Renal Physiol* 289: F850-62, 2005. https://doi.org/10.1152/ajprenal.00011.2005.
- B26 41. D'Souza S, Garcia-Cabado A, Yu F, Teter K, Lukacs G, Skorecki K, Moore HP,
   B27 Orlowski J, Grinstein S. The epithelial sodium-hydrogen antiporter Na+/H+ exchanger 3
   B28 accumulates and is functional in recycling endosomes. *J Biol Chem* 273: 2035–2043,
   B29 1998. https://doi.org/10.1074/jbc.273.4.2035.
- Orlowski J, Grinstein S. Emerging roles of alkali cation/proton exchangers in organellar homeostasis. *Curr Opin Cell Biol* 19: 483–492, 2007.
   https://doi.org/10.1016/j.ceb.2007.06.001.
- Onishi A, Fu Y, Patel R, Darshi M, Crespo-Masip M, Huang W, Song P, Freeman B, Kim YC, Soleimani M, Sharma K, Thomson SC, Vallon V. A role for tubular Na+/H+ exchanger NHE3 in the natriuretic effect of the SGLT2 inhibitor empagliflozin. *Am J Physiol Renal Physiol* 319: F712–F728, 2020. https://doi.org/10.1152/ajprenal.00264.2020.
- Kocinsky HS, Dynia DW, Wang T, Aronson PS. NHE3 phosphorylation at serines 552
   and 605 does not directly affect NHE3 activity. *Am J Physiol Renal Physiol* 293: F212-8,
   2007. https://doi.org/10.1152/ajprenal.00042.2007.
- Krajoinas RO, Lessa LMA, Carraro-Lacroix LR, Davel APC, Pacheco BPM, Rossoni LV, Malnic G, Girardi ACC. Posttranslational mechanisms associated with reduced NHE3 activity in adult vs. young prehypertensive SHR. Am J Physiol Renal Physiol 299: F872-81, 2010. https://doi.org/10.1152/ajprenal.00654.2009.

Dalle Pezze P, Ruf S, Sonntag AG, Langelaar-Makkinje M, Hall P, Heberle AM,
 Razquin Navas P, van Eunen K, Tölle RC, Schwarz JJ, Wiese H, Warscheid B,
 Deitersen J, Stork B, Fäßler E, Schäuble S, Hahn U, Horvatovich P, Shanley DP,
 Thedieck K. A systems study reveals concurrent activation of AMPK and mTOR by
 amino acids. Nat Commun 7: 13254, 2016. https://doi.org/10.1038/ncomms13254.

- Secker PF, Beneke S, Schlichenmaier N, Delp J, Gutbier S, Leist M, Dietrich DR.
   Canagliflozin mediated dual inhibition of mitochondrial glutamate dehydrogenase and complex I: an off-target adverse effect. *Cell Death Dis* 9: 226, 2018.
   https://doi.org/10.1038/s41419-018-0273-y.
- Fontaine E. Metformin-Induced Mitochondrial Complex I Inhibition: Facts, Uncertainties, and Consequences. *Front Endocrinol (Lausanne)* 9: 753, 2018. https://doi.org/10.3389/fendo.2018.00753.
- Teeter ME, Baginsky ML, Hatefi Y. Ectopic inhibition of the complexes of the electron transport system by rotenone, piericidin A, demerol and antimycin A. *Biochim Biophys Acta* 172: 331–333, 1969. https://doi.org/10.1016/0005-2728(69)90076-0.
- 860 50. Billing AM, Kim YC, Gullaksen S, Schrage B, Raabe J, Hutzfeldt A, Demir F,
   861 Kovalenko E, Lassé M, Dugourd A, Fallegger R, Klampe B, Jaegers J, Li Q,
   862 Kravtsova O, Crespo-Masip M, Palermo A, Fenton RA, Hoxha E, Blankenberg S,
   863 Kirchhof P, Huber TB, Laugesen E, Zeller T, Chrysopolou M, Saez-Rodriguez J,
   864 Magnussen C, Eschenhagen T, Staruschenko A, Siuzdak G, Poulsen PL, Schwab C,
   865 Cuello F, Vallon V, Rinschen MM. Metabolic communication by SGLT2 inhibition.
- Niu Y, Liu R, Guan C, Zhang Y, Chen Z, Hoerer S, Nar H, Chen L. Structural basis of inhibition of the human SGLT2-MAP17 glucose transporter. *Nature* 601: 280–284, 2022. https://doi.org/10.1038/s41586-021-04212-9.
- Grahammer F, Huber TB, Artunc F. Role of mTOR Signaling for Tubular Function and
   Disease. *Physiology (Bethesda)* 36: 350–358, 2021.
   https://doi.org/10.1152/physiol.00021.2021.
- Grahammer F, Ramakrishnan SK, Rinschen MM, Larionov AA, Syed M, Khatib H,
   Roerden M, Sass JO, Helmstaedter M, Osenberg D, Kühne L, Kretz O, Wanner N,
   Jouret F, Benzing T, Artunc F, Huber TB, Theilig F. mTOR Regulates Endocytosis and
   Nutrient Transport in Proximal Tubular Cells. J Am Soc Nephrol 28: 230–241, 2017.
   https://doi.org/10.1681/ASN.2015111224.
- Zaccardi F, Webb DR, Htike ZZ, Youssef D, Khunti K, Davies MJ. Efficacy and safety of sodium-glucose co-transporter-2 inhibitors in type 2 diabetes mellitus: systematic review and network meta-analysis. *Diabetes Obes Metab* 18: 783–794, 2016. https://doi.org/10.1111/dom.12670.
- McGuire DK, Shih WJ, Cosentino F, Charbonnel B, Cherney DZI, Dagogo-Jack S,
   Pratley R, Greenberg M, Wang S, Huyck S, Gantz I, Terra SG, Masiukiewicz U,
   Cannon CP. Association of SGLT2 Inhibitors With Cardiovascular and Kidney Outcomes in Patients With Type 2 Diabetes: A Meta-analysis. *JAMA Cardiol* 6: 148–158, 2021. https://doi.org/10.1001/jamacardio.2020.4511.
- Fala L. Invokamet (Canagliflozin plus Metformin HCI): First Fixed-Dose Combination with an SGLT2 Inhibitor Approved for the Treatment of Patients with Type 2 Diabetes. *Am Health Drug Benefits* 8: 70–74, 2015.

- Goldman JD. Combination of empagliflozin and metformin therapy: A consideration of its place in type 2 diabetes therapy. *Clin Med Insights Endocrinol Diabetes* 11: 1179551418786258, 2018. https://doi.org/10.1177/1179551418786258.
- Sen T, Heerspink HJL. A kidney perspective on the mechanism of action of sodium glucose co-transporter 2 inhibitors. *Cell Metab* 33: 732–739, 2021.
   https://doi.org/10.1016/j.cmet.2021.02.016.
- de Albuquerque Rocha N, Neeland IJ, McCullough PA, Toto RD, McGuire DK.
   Effects of sodium glucose co-transporter 2 inhibitors on the kidney. *Diab Vasc Dis Res* 375–386, 2018. https://doi.org/10.1177/1479164118783756.
- Layton AT, Vallon V, Edwards A. Predicted consequences of diabetes and SGLT inhibition on transport and oxygen consumption along a rat nephron. *Am J Physiol Renal Physiol* 310: F1269-83, 2016. https://doi.org/10.1152/ajprenal.00543.2015.
- 901 61. Chen X, Hu P, Vaccaro N, Polidori D, Curtin CR, Stieltjes H, Sha S, Weiner S, Devineni D. Pharmacokinetics, Pharmacodynamics, and Safety of Single-Dose Canagliflozin in Healthy Chinese Subjects. *Clin Ther* 37: 1483-1492.e1, 2015. https://doi.org/10.1016/j.clinthera.2015.04.015.
- 905 62. **Devineni D, Curtin CR, Polidori D, Gutierrez MJ, Murphy J, Rusch S, Rothenberg**906 **PL**. Pharmacokinetics and pharmacodynamics of canagliflozin, a sodium glucose cotransporter 2 inhibitor, in subjects with type 2 diabetes mellitus. *J Clin Pharmacol* 53: 601–610, 2013. https://doi.org/10.1002/jcph.88.
- 909 63. **Scheen AJ**. Pharmacodynamics, efficacy and safety of sodium-glucose co-transporter type 2 (SGLT2) inhibitors for the treatment of type 2 diabetes mellitus. *Drugs* 75: 33–59, 2015. https://doi.org/10.1007/s40265-014-0337-y.
- 912 64. Sokolov V, Yakovleva T, Chu L, Tang W, Greasley PJ, Johansson S, Peskov K,
   913 Helmlinger G, Boulton DW, Penland RC. Differentiating the Sodium-Glucose
   914 Cotransporter 1 Inhibition Capacity of Canagliflozin vs. Dapagliflozin and Empagliflozin Using Quantitative Systems Pharmacology Modeling. CPT Pharmacometrics Syst
   916 Pharmacol 9: 222–229, 2020. https://doi.org/10.1002/psp4.12498.
- 917 65. **Tahara A**, **Takasu T**, **Yokono M**, **Imamura M**, **Kurosaki E**. Characterization and comparison of sodium-glucose cotransporter 2 inhibitors in pharmacokinetics, pharmacodynamics, and pharmacologic effects. *J Pharmacol Sci* 130: 159–169, 2016. https://doi.org/10.1016/j.jphs.2016.02.003.
- Kakinuma H, Oi T, Hashimoto-Tsuchiya Y, Arai M, Kawakita Y, Fukasawa Y, Iida I, Hagima N, Takeuchi H, Chino Y, Asami J, Okumura-Kitajima L, Io F, Yamamoto D, Miyata N, Takahashi T, Uchida S, Yamamoto K. (1S)-1,5-anhydro-1-[5-(4-ethoxybenzyl)-2-methoxy-4-methylphenyl]-1-thio-D-glucitol (TS-071) is a potent, selective sodium-dependent glucose cotransporter 2 (SGLT2) inhibitor for type 2 diabetes treatment. *J Med Chem* 53: 3247–3261, 2010. https://doi.org/10.1021/jm901893x.
- Fu Y, Breljak D, Onishi A, Batz F, Patel R, Huang W, Song P, Freeman B, Mayoux E,
   Koepsell H, Anzai N, Nigam SK, Sabolic I, Vallon V. Organic anion transporter OAT3
   enhances the glucosuric effect of the SGLT2 inhibitor empagliflozin. *Am J Physiol Renal Physiol* 315: F386–F394, 2018. https://doi.org/10.1152/ajprenal.00503.2017.

- 931 68. **Oe Y, Vallon V**. The pathophysiological basis of diabetic kidney protection by inhibition of SGLT2 and SGLT1. *Kidney and Dialysis* 2: 349–368, 2022. https://doi.org/10.3390/kidneydial2020032.
- 934 69. **Tang J, Ye L, Yan Q, Zhang X, Wang L**. Effects of Sodium-Glucose Cotransporter 2 935 Inhibitors on Water and Sodium Metabolism. *Front Pharmacol* 13: 800490, 2022. 936 https://doi.org/10.3389/fphar.2022.800490.
- 70. Zinman B, Wanner C, Lachin JM, Fitchett D, Bluhmki E, Hantel S, Mattheus M,
   938 Devins T, Johansen OE, Woerle HJ, Broedl UC, Inzucchi SE, EMPA-REG OUTCOME Investigators. Empagliflozin, cardiovascular outcomes, and mortality in type 2 diabetes.
   N Engl J Med 373: 2117–2128, 2015. https://doi.org/10.1056/NEJMoa1504720.
- 941 71. **Guthrie R**. Canagliflozin and cardiovascular and renal events in type 2 diabetes.
   942 *Postgrad Med* 130: 149–153, 2018. https://doi.org/10.1080/00325481.2018.1423852.
- 943 72. **O'Neill J, Fasching A, Pihl L, Patinha D, Franzén S, Palm F**. Acute SGLT inhibition normalizes O2 tension in the renal cortex but causes hypoxia in the renal medulla in anaesthetized control and diabetic rats. *Am J Physiol Renal Physiol* 309: F227-34, 2015. https://doi.org/10.1152/ajprenal.00689.2014.
- 73. **Raghavan V, Rbaibi Y, Pastor-Soler NM, Carattino MD, Weisz OA**. Shear stress-dependent regulation of apical endocytosis in renal proximal tubule cells mediated by primary cilia. *Proc Natl Acad Sci U S A* 111: 8506–11, 2014.
- 74. Wang T, Weinbaum S, Weinstein AM. Regulation of glomerulotubular balance: flow-activated proximal tubule function. *Pflugers Arch* 469: 643–654, 2017.
   https://doi.org/10.1007/s00424-017-1960-8.
- 953
   75. Watts NB, Bilezikian JP, Usiskin K, Edwards R, Desai M, Law G, Meininger G.
   954 Effects of canagliflozin on fracture risk in patients with type 2 diabetes mellitus. *J Clin Endocrinol Metab* 101: 157–166, 2016. https://doi.org/10.1210/jc.2015-3167.
- 956 76. Shipman KE, Baty CJ, Long KR, Rbaibi Y, Cowan IA, Gerges M, Marciszyn AL,
  957 Kashlan OB, Tan RJ, Edwards A, Weisz OA. Impaired endosome maturation mediates
  958 tubular proteinuria in dent disease cell culture and mouse models. *J Am Soc Nephrol* 34:
  959 619–640, 2023. https://doi.org/10.1681/ASN.000000000000084.
- Pesta D, Gnaiger E. High-resolution respirometry: OXPHOS protocols for human cells and permeabilized fibers from small biopsies of human muscle. *Methods Mol Biol* 810: 25–58, 2012. https://doi.org/10.1007/978-1-61779-382-0 3.

Table I. Single dose effects of canagliflozin and empagliflozin in mice.

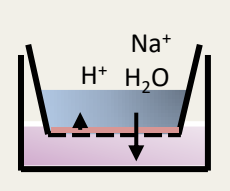
	Baseline (normalized)	Empagliflozin- treated (norm to baseline)	Baseline (normalized)	Canagliflozin- treated (norm to baseline)	P value cana vs empa
Water intake/24h	100+/-35.9	138.5+/-63.8	100+/-27.8	144+/-44.3	NS (0.996)
Urine output/24h	100+/-54.7	194+/-88.8 ****	100+/-63.6	409+/-201 ****	* (0.03)
Albumin/24h	100+/-31.0	172+/-67.8 ***	100+/-60.8	214+/-96.1 ***	NS (0.699)
Creatinine/24h	100+/-39.0	180+/-78.6 ***	100+/-60.6	229+/-116 ***	NS (0.710)
Albumin/Creatinine	100+/-25.6	92.9+/-21.5	100+/-32/3	96.6+/-25.4	NS (0.995)

<sup>\*\*\*</sup>P<0.001, \*\*\*\*p<0.0001 vs baseline by two-way ANOVA with Tukey's multiple comparisons test. All baseline comparisons NS except urine output p 0.03. n=12 mice per condition, two trials per mouse.

# Canagliflozin but not empagliflozin inhibits Na\*-dependent fluid transport and endocytosis in proximal tubule cells

# **METHODS**

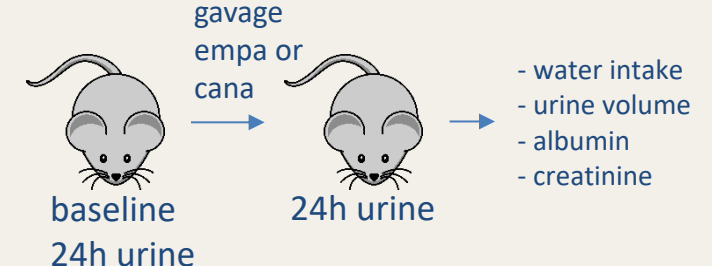
Quantitation of transport, acidification, endocytosis, and mitochondrial respiration in differentiated PT cell culture model





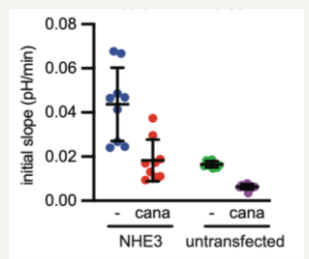


Single dose administration of gliflozins in mice

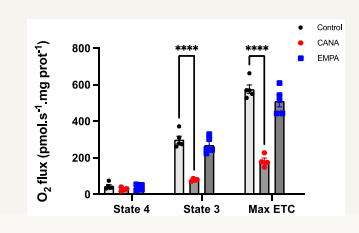


# **OUTCOME**

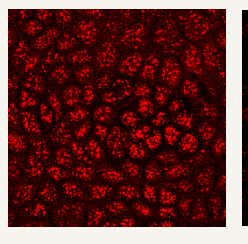
Canagliflozin inhibits surface NHE3

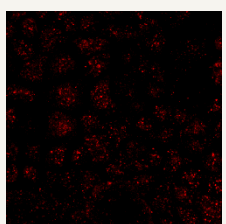


Canagliflozin inhibits mitochondrial complex I

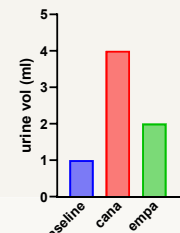


Canagliflozin inhibits albumin uptake in PT cells



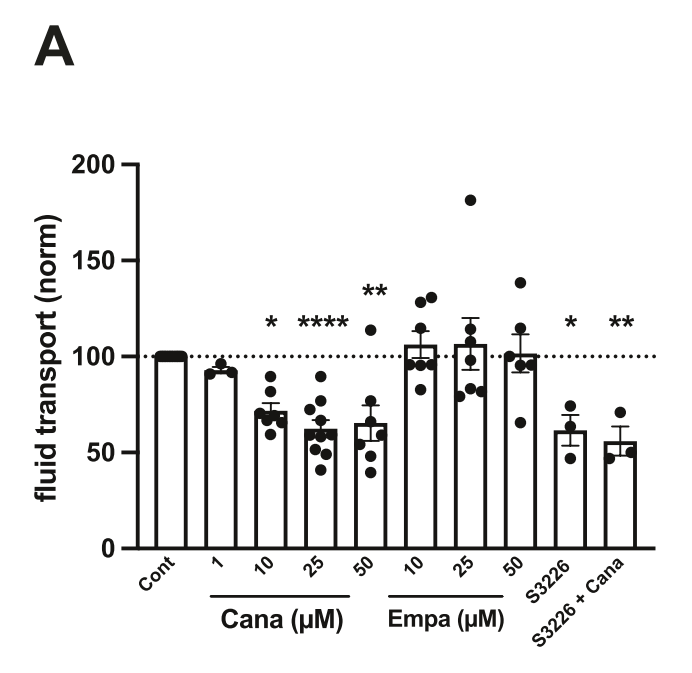


Canagliflozin-dosed mice have increased urine volume compared with empaglifozin-treated mice



**CONCLUSION** Canagliflozin rapidly inhibits surface NHE3 and mitochondrial complex I activity in proximal tubule cells, resulting in reduced fluid transport and endocytic uptake.

В



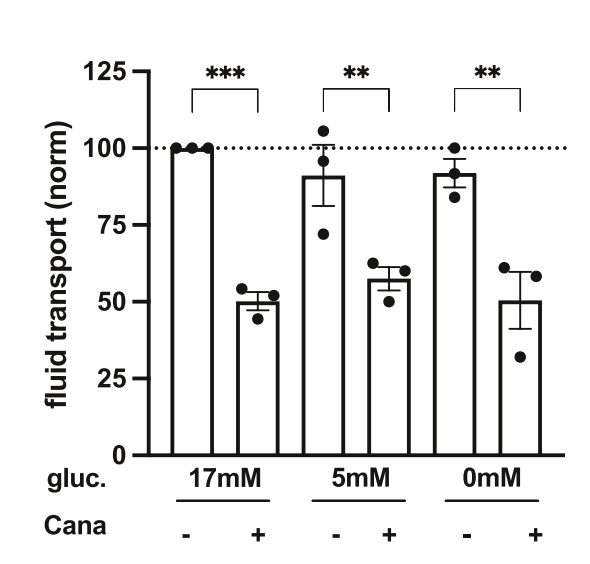


Figure 2

